Journal of Materials Chemistry C

RSC Publishing

PAPER

View Article Online
View Journal | View Issue

Cite this: J. Mater. Chem. C, 2013, 1, 5843

Melilite-type blue chromophores based on Mn^{3+} in a trigonal-bipyramidal coordination induced by interstitial oxygen†

Tae-Gon Kim,*[a] Seung-Joo Kim,[b] Chun Che Lin,[c] Ru-Shi Liu,*[c] Ting-Shan Chan[d] and Seoung-Jae Im[a]

Received 27th April 2013
Accepted 24th July 2013

DOI: 10.1039/c3tc30795f

www.rsc.org/MaterialsC

A new, earth-abundant, environmentally benign, and stable inorganic blue chromophore series $Sr_2(Mg_{1-x}Mn_x)Ge_2O_{7+\delta}$ has been prepared and characterized by X-ray absorption spectroscopy, synchrotron X-ray diffraction, and *ab initio* total energy calculation. As the content of Mn in the compound was increased, the color changed from white (for $x = 0.0$) to sky blue, deep blue, and finally black body color (for $x = 1.0$). $Sr_2MgGe_2O_7$ has the melilite-type structure comprising $Mg(2+)O_4$ and GeO_4 tetrahedra. On the other hand, it was found that the Mn ion in $Sr_2(Mg_{1-x}Mn_x)Ge_2O_{7+\delta}$ is mainly trivalent and that the additional oxygen atom infiltrates into the lattice to compensate for the excess positive charge. The additional oxygen atom occupies an interstitial site, leading to the formation of $Mn(3+)O_5$ trigonal bipyramid and $Ge(4+)O_5$ square pyramid. As the driving force for the $Mn(3+)O_5$ formation, the tendency for improving the lattice coherency between BO_4–$B'O_4$ and AO_8 layers in the melilite $A_2BB'_2O_7$ is suggested.

1 Introduction

Rich blue pigments, which are used for art and decorative purposes, were rare and expensive before the industrial revolution. Owing to significant efforts to find low-cost blue pigments, several useful synthetic materials that are blue in color, such as Prussian blue ($Fe_4[Fe(CN)]_3 \cdot xH_2O$) associated with the intervalence charge transfer from Fe^{2+} to Fe^{3+}, French ultramarine ($Na_7Al_6Si_6O_{24}S_3$) based on the absorption in thiozonide anion S_3^-, Cobalt blue ($CoAl_2O_4$) and Cerulean blue ($CoO \cdot nSnO_2$) attributed to the allowed d–d transition in the Co^{2+} ion, have been developed since the 18th century.[1–4] Even though these materials exhibit good color properties and relatively low costs – they are typically less expensive than the natural gemstone lapis lazuli – their toxicity or insufficient durability continue to be issues. Recently, the synthesis of blue-chromophore oxides including a Mn^{3+} ion in the trigonal-bipyramidal coordination was reported as a new route for developing earth-abundant, environmentally benign, and stable inorganic blue pigments.[5] The blue color originates from green/red-range absorption by a symmetry-allowed optical transition between Mn $3d_{x^2-y^2,xy}$ and Mn $3d_{z^2}$ states in the coordination. Their color hue can be finely tuned by the types and compositions of the hosts.[6,7] However, few host structures having a Mn^{3+} ion in their geometry have been found so far. Most of them have hexagonal $YInO_3$-, $YbFe_2O_4$-, and $LuFeO_3(ZnO)_2$-type structures, where Mn^{3+} is partially substituted in the In^{3+} or Fe^{3+} sites.[5–7] This is primarily due to the instability of five coordinated Mn^{3+} ions in the trigonal-bipyramidal geometry.[8] In this study, we synthesized a new blue chromophore, $Sr_2(Mg,Mn)Ge_2O_{7+\delta}$, which has a melilite-related structure. It has been known that the melilite-type compounds with a general formula $Sr_2MGe_2O_7$ (M = Mg, Zn, Co, Mn) consist of M^{2+} and Ge^{4+} in tetrahedral coordinations without excess oxygen for more than 30 years.[9–11] On the basis of X-ray absorption spectroscopy measurements, synchrotron X-ray diffraction analysis, and *ab initio* total energy calculation, however, we revealed the existence of an Mn^{3+} ion in a trigonal-bipyramidal coordination and Ge^{4+} in a square-pyramidal coordination induced by the infiltrated oxygen interstitial in $Sr_2(Mg,Mn)Ge_2O_{7+\delta}$. It was unexpected that Mn^{3+} ions substituted in MgO_4 tetrahedral sites have a trigonal-bipyramidal coordination, since other hosts for blue chromophores based on Mn^{3+} ions have originally trivalent trigonal-bipyramidal sites, such as $In(3+)O_5$, $Ga(3+)O_5$, $Fe(3+)O_5$, *etc.*[5–7] It

[a]Electronics Material Laboratory, Samsung Advanced Institute of Technology, Yongin, Korea. E-mail: taegon2.kim@samsung.com

[b]Department of Chemistry, Division of Energy Systems Research, Ajou University, Suwon, Korea

[c]Department of Chemistry, National Taiwan University, Taipei 106, Taiwan. E-mail: rsliu@ntu.edu.tw

[d]National Synchrotron Radiation Research Center, Hsinchu 300, Taiwan

† Electronic supplementary information (ESI) available: Conventional X-ray powder diffraction patterns, Mn L-edge spectra fitting by the linear combination of references, synchrotron X-ray diffraction patterns, two tables listing the refined crystallographic data, a table listing the calculated crystal structure, a table listing the selected bond distances in the calculated crystal structure, partial density of states, and a scheme describing the stability of the layered melilite structure on the basis of the interlayer coherency model. See DOI: 10.1039/c3tc30795f

is suggested that the five coordinations around Mn^{3+} and Ge^{4+} ions might result from the oxidation of Mn^{2+} ions owing to the uptake of an additional oxygen atom.

2 Experimental section

$Sr_2(Mg_{1-x}Mn_x)Ge_2O_7$ ($x = 0.0$, 0.1, 0.2, 0.3, 0.4, 0.5, 0.6, 0.8, and 1.0) were prepared using solid-state reaction. Stoichiometric amounts of $SrCO_3$ (Aldrich, 99.995%), MgO_2 (Aldrich, 99.99%), $MnCO_3$ (Aldrich, 99.99%), and GeO_2 (Kojundo, 99.99%) were homogeneously mixed. The mixtures were fired at 1250 °C for 6 h under ambient conditions. Optical absorption of the resultants was measured with a UV-VIS absorption spectroscope with an integrating sphere (Hitachi U-3310). Phase information was obtained by using a normal X-ray diffraction with $\lambda = 1.540562$ Å (XRD, Phillips X′Pert Pro, Target Cu Kα, 40 kV, 40 mA).

Synchrotron X-ray powder diffraction experiments were performed using a multiple detector system installed at the 8C2 beamline of the Pohang Light Source, Pohang Accelerator Laboratory in Korea. A monochromatic 1.549 Å X-ray beam was used. Diffraction data were collected over the 2θ range of 10–130° with a step of 0.005° in asymmetric flat-specimen reflection geometry with a fixed angle of 7.0° at room temperature. Rietveld refinement was carried out using the Rietan-2000 package.[12] Whole-pattern fitting based on the maximum entropy method (MEM) was carried out using the computer program PRIMA47 with 160 × 160 × 100 pixels. VESTA (ver. 3.0.3) was used to draw the electron density maps from the MEM analysis.

The X-ray absorption near-edge structure (XANES) and extended X-ray absorption fine structure (EXAFS) spectra at the Mn K-edge were recorded in transmission mode with a wiggler 17C1beamline at the National Synchrotron Radiation Research Center (NSRRC) in Taiwan. XANES spectra at Mn $L_{2,3}$-edges and the O K-edge were obtained at the BL20A beamline in total electron yield (TEY) mode.

The first-principles calculations based on the density functional theory (DFT)[13] were performed using *Vienna Ab initio Simulation Package* (VASP) code to estimate the density of states.[14,15] The plane-wave cutoff energy was chosen to be 400 eV and the *k*-points were sampled on 4 × 4 × 6 uniform grids. The exchange–correlation interactions between electrons were described by generalized gradient approximation (GGA),[16] and the projector-augmented wave (PAW) potentials[14,15] were used to describe the ion–electron interactions. The conjugate gradient method for geometry optimization was used. The optimization procedure was truncated when the residual forces for the relaxed atoms were less than 0.01 eV $Å^{-1}$.

3 Results and discussion

The Mn-substituted melilite-type $Sr_2MgGe_2O_7$ exhibited blue color, as shown in Fig. 1(a). As the amount of Mn substituted in the compound was increased, the color changed from white to sky blue, blue, and then deep blue. In its final composition, $Sr_2MnGe_2O_7$ shows black body color. Fig. 1(b) shows the optical

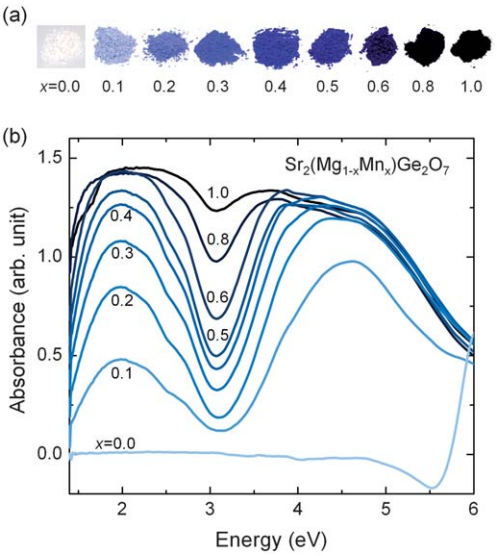

Fig. 1 (a) Colors and (b) absorption spectra of $Sr_2(Mg_{1-x}Mn_x)Ge_2O_7$ ($x = 0.0$, 0.1, 0.2, 0.3, 0.4, 0.5, 0.6, 0.8, and 1.0) powders.

absorption spectra of $Sr_2(Mg_{1-x}Mn_x)Ge_2O_7$ ($x = 0.0$, 0.1, 0.2, 0.3, 0.4, 0.5, 0.6, 0.8, and 1.0). The optical bandgap of $Sr_2MgGe_2O_7$ without Mn was estimated to be 5.6 eV, and two absorption bands appeared in the energy range of 1.6–2.8 eV and 3.5–6.0 eV by the Mn substitution. The blue hue of the compound was attributed to absorption in the visible light range, *i.e.*, absorption at 1.6–2.8 eV. As the Mn concentration was increased, the relative absorption intensities increased and so did the widths of the two bands. This change is manifested in the form of changes in the color which increased in vividness and depth and ultimately became black (Fig. 1(a)).

The structural change induced by the substitution of Mg with Mn was checked using X-ray diffraction (XRD) analysis (Fig. S1†). The overall crystallographic structure with a $P\bar{4}2_1m$ space group was maintained for all Mn concentrations. This meant that Mn was incorporated into the MgO_4 tetrahedron site in the $Sr_2MgGe_2O_7$ structure. In the case of the successful substitution of Mn^{2+} for Mg^{2+}, one can expect a gradual increase in the volume of the unit cell due to the fact that the Mn^{2+} ion (80 pm) is 13% larger than the Mg^{2+} ion (71 pm).[17] However, in reality, the cell volume decreased with an increase in the Mn concentration as shown in Fig. 2. Shrinkage along the *a*-axis was more dominant than the expansion along the *c*-axis. Hence, the decrease in the unit cell volume implied that the substitution would be more complex change than Mg^{2+} ions merely be replaced by Mn^{2+} at the site.

In general, the d–d transition of a high spin Mn^{2+} (d^5) ion in a tetrahedral coordination does not result in such a strong optical absorption. This is due to the spin-forbidden character of the transition.[18] In addition, the absorption attributable to the charge transfer from the O 2p level to the Mn 3d level does not occur in the visible-light range. Hence, the 2+ oxidation state of Mn was investigated more closely. Fig. 3(a) shows the L-edge X-ray absorption near-edge structure (XANES) spectra of Mn originating from an electric dipole-allowed 2p → 3d transition in $Sr_2(Mg_{0.6}Mn_{0.4})Ge_2O_7$ and $Sr_2MnGe_2O_7$.

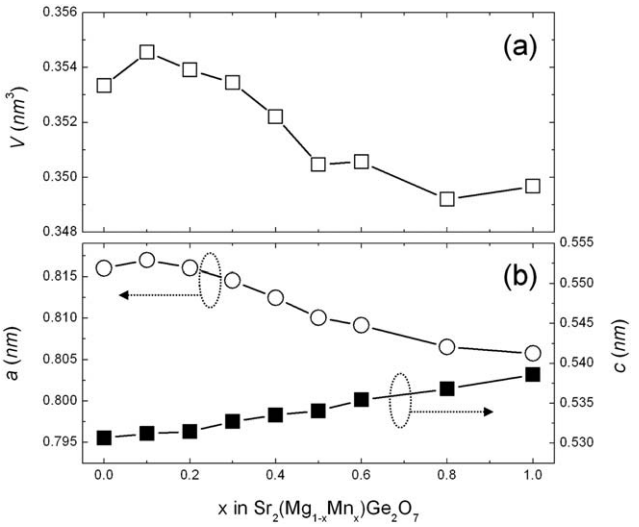

Fig. 2 (a) Unit cell volumes and (b) lattice parameters of $Sr_2(Mg_{1-x}Mn_x)Ge_2O_7$ (x = 0.0, 0.1, 0.2, 0.3, 0.4, 0.5, 0.6, 0.8 and 1.0) powders.

MnO(2+), Mn_2O_3(3+), and MnO_2(4+) were used as the reference samples. L_3-absorption edges of two samples show the linear combination of the L_3-edges of MnO(2+) and Mn_2O_3(3+) (Fig. S2†),[19,20] and the relative intensity of the characteristic peak of MnO(2+) is smaller in $Sr_2MnGe_2O_7$ than in $Sr_2(Mg_{0.7}Mn_{0.3})Ge_2O_7$. That is, the Mn ions in both samples have mixed oxidation states of 2+/3+, and the oxidation state of Mn in $Sr_2MnGe_2O_7$ is closer to 3+ than in $Sr_2(Mg_{0.6}Mn_{0.4})Ge_2O_7$. The mixed oxidation states of Mn are noticed from the positions of the Mn K-edge (1s → 4p) at around 6550 eV (Fig. 3(b)) and the characteristic pre-peak shoulder in the O K-edge (1s → 2p) at around 531 eV (Fig. 3(c)) as well. The average oxidation states of $Sr_2(Mg_{0.6}Mn_{0.4})Ge_2O_7$ and $Sr_2MnGe_2O_7$ were quantitatively estimated from a linear dependence of Mn K-edge positions on the formal Mn valences from the reference samples, and were found to be 2.54 and 2.62, respectively (inset of Fig. 3(b)).[21] The edge positions were determined from the first inflection point of the XANES spectra. As can be seen from the extended X-ray absorption fine structure (EXAFS) spectra (Fig. 3(d)), the average bond distances between the Mn and O atoms in $Sr_2(Mg_{0.6}Mn_{0.4})Ge_2O_7$ and $Sr_2MnGe_2O_7$ (153 pm) were smaller than those in the case of $Sr_3MnGe_2O_8$ (184 pm) composed of only Mn^{2+} ions. This result also supported the conclusion that the oxidation state of Mn is mixed and close to 3+. Therefore, it would be reasonable to assume that the blue color was the result of absorption by Mn^{3+}, rather than by Mn^{2+} which is optically inert to visible light.

When Mn^{3+} ions are present in the melilite-type structure, there should be concomitant deviations in the known structure. This is due to the following two reasons. First, to compensate for the excess positive charge caused by the presence of a Mn^{3+} ion at a Mg^{2+} site ($Mn_{Mg}^{\cdot}$), either other cation vacancies ($V_{Sr}^{//}$ or $V_{Ge}^{////}$) or an additional anion ($O_i^{//}$) should be formed. Second, Mn^{3+} ions (d^4) in a tetrahedral coordination are energetically unfavorable owing to the Jahn–Teller distortion and, to our knowledge, have never been reported previously.[22] To reduce the energy of the system, the coordination around the Mn^{3+} ions should have a distribution different from that around Mn^{2+} ions. The Rietveld refinement of the synchrotron XRD patterns on the basis of the known structure model[9] gave extremely high

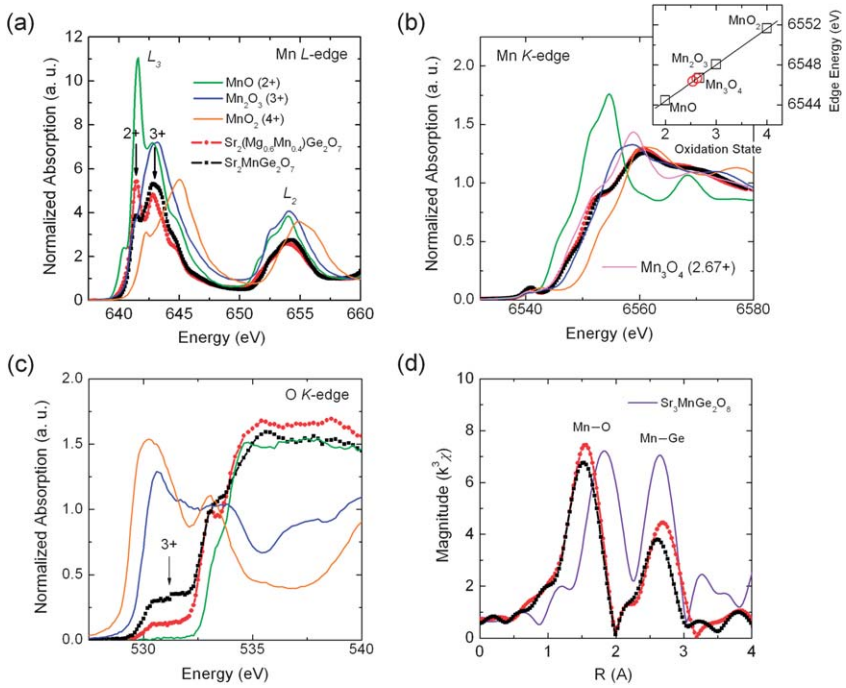

Fig. 3 (a) Mn L-edge, (b) Mn K-edge, and (c) O K-edge XANES, and (d) Fourier transformed EXAFS spectra of $Sr_2(Mg_{0.6}Mn_{0.4})Ge_2O_7$ and $Sr_2MnGe_2O_7$. MnO(2+), Mn_3O_4(2.67+), Mn_2O_3(3+), and MnO_2(4+) were used as the reference samples for the XANES spectra, and $Sr_3MnGe_2O_8$(2+) for the EXAFS spectra. The inset in (b) is the oxidation state determination of $Sr_2(Mg_{0.6}Mn_{0.4})Ge_2O_7$ and $Sr_2MnGe_2O_7$ (vacant red circles) using the Mn K-edge shift of the reference Mn compounds (vacant black squares).

values of the displacement parameters of the Mn and O ions (Table S1†). This suggested that the actual structure might be slightly perturbed from the reference model around the Mn and O ions. From the electron mapping performed *via* an entropy maximum method (MEM)-based analysis, we could detect the trace of an additional oxygen (O_4) atom around (0.35, 0.42, and 0.19) as shown in Fig. 4. However, the refinement simply including an O_4 atom at the 8f site in the unit cell also did not reduce the large displacement parameters despite the slight improvement of reliability factors from $R_{wp} = 10.06$, $R_p = 7.75$, and $S = 1.15$ to $R_{wp} = 9.31$, $R_p = 7.18$, and $S = 1.07$ (Table S2†). The complex split of atomic positions induced by partial occupation of the interstitial atoms could not be clearly refined, because the atomic displacement is reflected just in the broadening of diffraction peaks without the distinct peak separation. Accordingly, we could not help estimating only the average position of component atoms with considerable inaccuracy. Nevertheless, it is noteworthy that the interstitial O_4 plausibly changes the coordination around the Mn^{3+} ion, and compensates for the excess positive charge that results from the presence of the Mn^{3+} ion. Breaking of the tetrahedral coordination around Mn ions can be experimentally supported also by the pre-edge peak intensities of Mn K-edge XANES spectra. Fig. 5 shows the pre-edge peaks from $Sr_2(Mg_{0.6}Mn_{0.4})Ge_2O_7$, $Sr_2MnGe_2O_7$, and $MnFe_2O_4$, as a reference, with 85% Mn^{2+} in tetrahedral sites and 15% Mn^{2+} in octahedral sites. Integrated intensities of the pre-edge peaks from $Sr_2(Mg_{0.6}Mn_{0.4})Ge_2O_7$ and $Sr_2MnGe_2O_7$ are just about 59% and 63% of $MnFe_2O_4$, respectively. The smaller pre-edge peaks suggest that the local symmetry around Mn in both samples might have a higher-fold coordination than a 4-fold tetrahedral coordination. This is consistent with the structure estimated from the synchrotron XRD.

Since the experiments using the synchrotron XRD and XANES analysis were not enough to validate the interstitial inclusion and to understand its detailed contribution to the crystal structure, we tried to estimate the thermodynamic probability of the system on the basis of the density functional theory (DFT). The formation energy of interstitial oxygen ($\Delta E(O_i)$) was calculated through the following equation.

$$\Delta E(O_i) = E_{tot}(O_i) - E^0_{tot} - \mu_O,$$

where $E_{tot}(O_i)$ and E^0_{tot} are the total energies of the supercells with ($Sr_2MnGe_2O_{7.5}$) and without interstitial oxygen O_i ($Sr_2MnGe_2O_7$), respectively, and μ_O is the chemical potential of O calculated on the basis of the O_2 molecule. Using the calculated values of $E_{tot}(O_i)$, E^0_{tot}, and μ_O, which were −172.27 eV, −164.78 eV, and −4.93 eV, respectively, the energy of formation of an interstitial oxygen atom was found to be −2.56 eV. The inclusion of the additional oxygen atom reduces the total energy of the system, *i.e.* $Sr_2MnGe_2O_{7.5}$ is energetically more stable than $Sr_2MnGe_2O_7$. The calculated crystal structures of $Sr_2MnGe_2O_7$ and $Sr_2MnGe_2O_{7.5}$ are shown in Fig. 6(a) and (b). (The atomic positions and selected bond distances of $Sr_2MnGe_2O_{7.5}$ are listed in Tables S3 and S4,† respectively.) The location of the interstitial oxygen atom (0.55, 0.29, and 0.78) is consistent with that estimated through the MEM and the refinement of the synchrotron XRD patterns as (0.58, 0.34, and 0.82). The interstitial atom between MnO_4 and GeO_4 pushes the adjacent oxygen atoms and transforms the corner-shared MnO_4–GeO_4–MnO_4 unit into the edge-shared MnO_5–GeO_5–MnO_5 unit as shown in Fig. 6(c) and (d). All the MnO_4

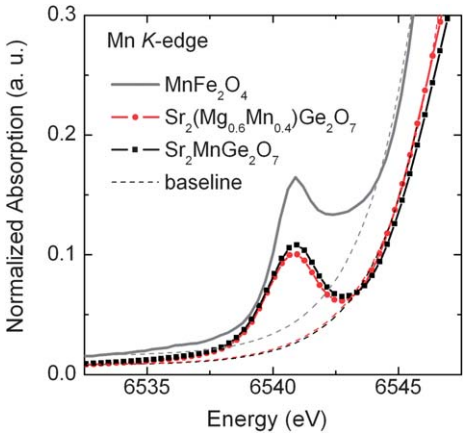

Fig. 5 Pre-edge peaks from $Sr_2(Mg_{0.6}Mn_{0.4})Ge_2O_7$, $Sr_2MnGe_2O_7$, and $MnFe_2O_4$ with a tetrahedral coordination around the Mn^{2+} ion. Baselines for estimating the integrated intensities are also plotted as dashed lines.

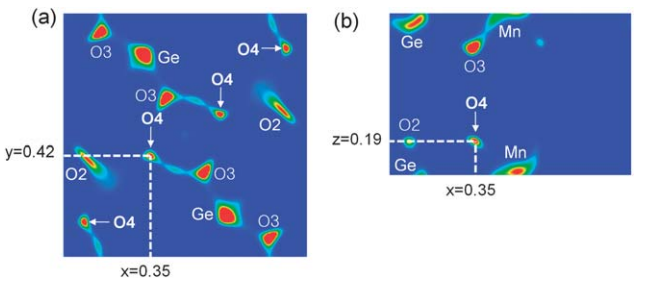

Fig. 4 Electron-scattering-density maps at the (a) $z = 0.19$ section of the (001) plane and (b) $y = 0.42$ section of the (010) plane, as determined from MEM analysis.

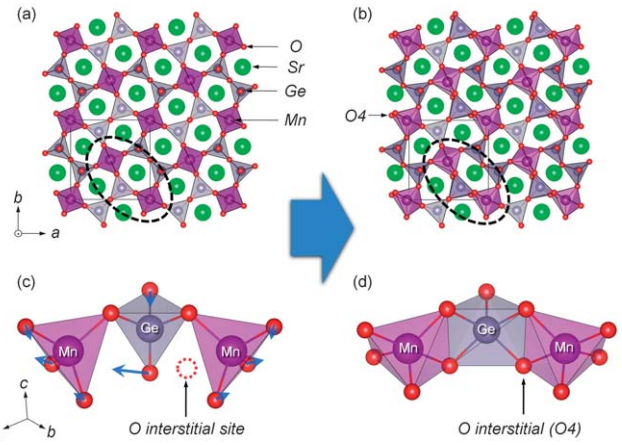

Fig. 6 Crystal structures of (a) $Sr_2MnGe_2O_7$ and (b) $Sr_2MnGe_2O_{7.5}$, where Sr, Mn, Ge, and O are denoted by the green, violet, bluish grey, and red spheres, respectively. The polyhedral blocks, MnO_4–GeO_4–MnO_4 and MnO_5–GeO_5–MnO_5, are represented by the dashed black circles in (a) and (b) and are enlarged in (c) and (d), respectively. The expected displacement of the oxygen atoms by the interstitial oxygen atom is shown by the blue arrows in (c).

tetrahedrons and one-fourth of the GeO_4 tetrahedrons in the unit cell of $Sr_2MnGe_2O_7$ are transformed into MnO_5 distorted-trigonal bipyramids and GeO_5 square pyramids by the addition of one oxygen atom. Inclusion of an interstitial oxygen has been reported in the Ga-based melilite structure $La_{1+x}Sr_{1-x}Ga_2O_{7+x/2}$ (LSG) to compensate for the excess charge from the La/Sr ratio by Kuang *et al.*[23] They expected that the flexibility of the Ga_2O_4 tetrahedron at the 4e site with a non-bridging terminal oxygen might be the key condition for the interstitial binding. However, in $Sr_2(Mg,Mn)Ge_2O_{7+\delta}$, the interstitial O_4 is shared by MnO_4 at the 2a site as well as by GeO_4 at the 4e site. Non-bridging terminal oxygen might not be a critical factor for the interstitial uptake in $Sr_2(Mg,Mn)Ge_2O_{7+\delta}$ at least. Recent theoretical and experimental studies also pointed out that the interstitial oxygen atom is shared by both Ga_1 and Ga_2 in LSG rather than being bound only to Ga_2 at the 4e site.[24,25]

As determined by the results of spectroscopic analysis and *via* DFT calculations, the blue color of $Sr_2(Mg,Mn)Ge_2O_{7+\delta}$ can be attributed to the presence of Mn^{3+} ions in a distorted-trigonal bipyramidal coordination. This is similar to what is noticed in the case of $Y(In,Mn)O_3$, $Lu(Ga,Mn)MgO_4$, and $Lu(Ga,Mn)O_3(ZnO)_2$.[5–7] The calculated density of states (DOS) of the two Mn ions in $Sr_2MnGe_2O_{7.5}$ suggest that four levels among the five 3d orbitals in Mn are occupied and that optical absorption in the range of 1.6–2.8 eV would occur through the transitions $e'' \rightarrow a'$ and $e' \rightarrow a'$ as shown in Fig. 7(a). They correspond also to Mn L_3-edge absorption where the edge shoulder at around 641 eV and the peak maximum at around 634 eV in Fig. 3(a) match to e''/e' and a', respectively.[20] The opposite spin ordering in Mn1 and Mn2 was indicative of the antiferromagnetic property of the structure, which had a theoretical magnetic moment of 4 μ_B. On the other hand, in the case of $Sr_2MnGe_2O_7$, the Mn ions had fully occupied 3d orbitals and thus cannot show an optical transition in the d orbitals (Fig. 7(b)). Even though $Sr_2MnGe_2O_7$ also exhibited antiferromagnetic ordering, its theoretical magnetic moment was 5 μ_B. It has been reported recently that the experimentally determined magnetic moment of $Sr_2MnGe_2O_7$ was 3.99 μ_B.[10] This report was based on the crystal structure of $Sr_2MnGe_2O_7$ and suggested that the acquired magnetic moment was smaller than the theoretical value of 5 μ_B owing to the measurement being made at 2.5 K, which is close to the Néel temperature of $Sr_2MnGe_2O_7$ (4.4 K). However, we believe that the measured value of 3.99 μ_B is attributable to the intrinsic property of $Sr_2MnGe_2O_{7.5}$ rather than to the experimental error in the measurement.

On the basis of the optical absorption spectra of the melilite-type $A_2(B,Mn)B'_2O_7$ compounds with various A, B, and B′ ions, such as $(Sr_{0.9}Ca_{0.1})_2(Mg_{0.8}Mn_{0.2})Ge_2O_7$, $(Sr_{0.8}Ca_{0.2})_2(Mg_{0.8}Mn_{0.2})Ge_2O_7$, $Sr_2(Mg_{0.8}Mn_{0.2})Ge_2O_7$, $Ba_2(Mg_{0.8}Mn_{0.2})Ge_2O_7$, $Sr_2(Zn_{0.8}Mn_{0.2})Ge_2O_7$, $Sr_2(Mg_{0.6}Mn_{0.4})Ge_2O_7$, and $Sr_2(Mg_{0.6}Mn_{0.4})Si_2O_7$ as shown in Fig. 8 we could gain insight into the conditions for the occurrence of a Mn^{3+} ion in the melilite structure including a Mn atom. Among the various melilites, only $Ba_2(Mg_{0.8}Mn_{0.2})Ge_2O_7$ and $Sr(Mg_{0.6}Mn_{0.4})Si_2O_7$, in which the A cation is larger than Sr and the B′ cation is smaller than Ge, respectively, are not blue in color. This result suggests that the oxidation states of Mn in these melilites depend on the sizes of the component ions in the melilites, since their colorless appearance results from Mn^{2+} and not from Mn^{3+}. On the basis of this observation, we propose the following condition for the occurrence of a Mn^{3+} ion in $Sr_2MnGe_2O_{7.5}$. The $A_2BB'_2O_7$-type melilite structure consists of two layers: the AO_8-connected layer and the BO_4–$B'O_4$-connected layer. Because the two layers shares an oxygen atom, the horizontal size of a unit block in the BO_4–$B'O_4$ layer should be comparable to that of a unit block in the AO_8 layer, as is the case in heteroepitaxial bilayers. If the mismatch in the sizes of the unit blocks of the two layers is too large, the melilite structure would be energetically unstable. This can be expressed as the scheme shown in Fig. S6.† In $Sr_2Mn(2+)Ge_2O_7$, the $Mn(2+)O_4$–GeO_4 layer might be too large to be matched to the SrO_8 layer, because a Mn^{2+} ion (80 pm) is 12.6% larger than a Mg^{2+} ion (71 pm) in stable $Sr_2MgGe_2O_7$. However, if the Mn^{2+} ion is oxidized to the smaller Mn^{3+} ion (72 pm in the five coordination), the discrepancy between the two layers would decrease, and the total energy of the system could be reduced. This is shown schematically in Fig. 9. On the other hand, the BaO_8 layer in $Ba_2(Mg_{0.8}Mn_{0.2})Ge_2O_7$ is larger than the SrO_8 layer (Ba^{2+}: 156 pm, Sr^{2+}: 140 pm) and large enough to be matched to the $Mn(2+)O_4$–GeO_4 layer. In addition, the $Mn(2+)O_4$–SiO_4 layer in $Sr_2(Mg_{0.6}Mn_{0.4})Si_2O_7$ is smaller than the $Mn(2+)O_4$–GeO_4 layer

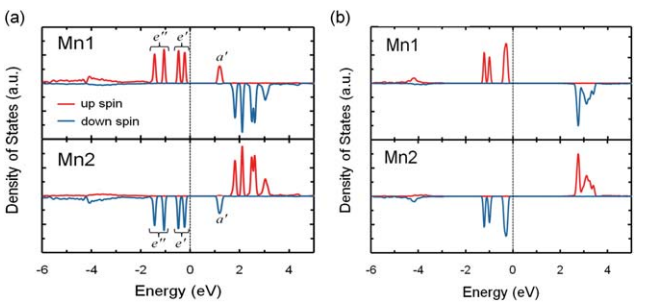

Fig. 7 Calculated partial density of states for Mn1 3d and Mn2 3d in (a) $Sr_2MnGe_2O_{7.5}$ and (b) $Sr_2MnGe_2O_7$. The Fermi level is set to zero.

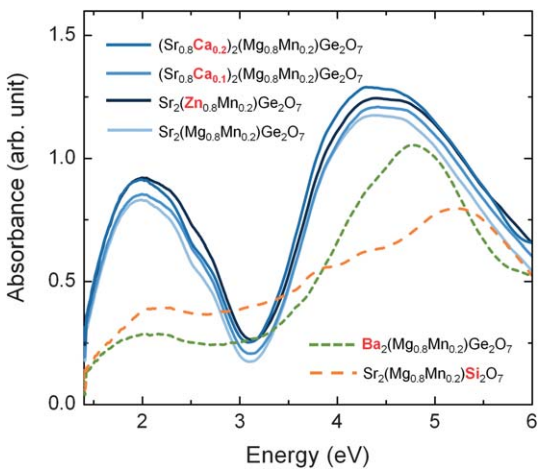

Fig. 8 Absorption spectra of the melilite $A_2(B,Mn)B'_2O_7$ with the various A, B, and B′ ions such as $(Sr_{0.9}Ca_{0.1})_2(Mg_{0.8}Mn_{0.2})Ge_2O_7$, $(Sr_{0.8}Ca_{0.2})_2(Mg_{0.8}Mn_{0.2})Ge_2O_7$, $Sr_2(Mg_{0.8}Mn_{0.2})Ge_2O_7$, $Ba_2(Mg_{0.8}Mn_{0.2})Ge_2O_7$, $Sr_2(Zn_{0.8}Mn_{0.2})Ge_2O_7$, $Sr_2(Mg_{0.8}Mn_{0.2})Ge_2O_7$, and $Sr_2(Mg_{0.8}Mn_{0.2})Si_2O_7$.

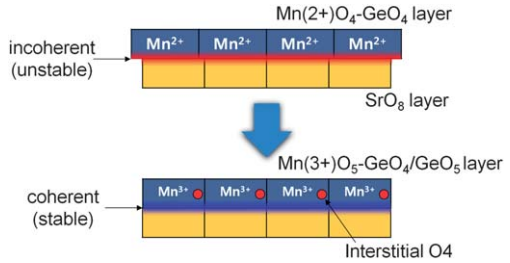

Fig. 9 Schematic description of the structural stabilization induced by the reduction in the interlayer mismatch in the layered $Sr_2MnGe_2O_{7.5}$ owing to the oxidation of $Mn(2+)O_4$–GeO_4 to $Mn(3+)O_5$–GeO_4/GeO_5.

(Si^{4+}: 40 pm, Ge^{4+}: 53 pm) and small enough to be similar to the SrO_8 layer. Hence, neither of the two compounds is blue in color and neither of them contain a Mn^{2+} ion instead of a Mn^{3+} ion. In brief, the valence states and the coordination in melilite-type structures could be determined on the basis of the degree of mismatch in the sizes of the AO_8 and BO_4–$B'O_4$ layers in the structures. It should be noted here that not all the Mn ions in $Sr_2(Mg,Mn)Ge_2O_{7+\delta}$ need to be of the Mn^{3+} type, and that this is the case only if coherency between the AO_8 and BO_4–$B'O_4$ layers is attained. The result that the mixed valence states of the Mn ions in $Sr_2(Mg_{0.6}Mn_{0.4})Ge_2O_{7+\delta}$ and $Sr_2MnGe_2O_{7+\delta}$ are 2.54 and 2.62 can be attributed to this reason.

4 Conclusions

In summary, the blue chromophore $Sr_2(Mg,Mn)Ge_2O_{7+\delta}$, which has a melilite-type structure, was firstly synthesized. On the basis of the results of X-ray absorption spectroscopy, synchrotron X-ray diffraction analysis, and *ab initio* calculations, it was found that the crystal structure of $Sr_2(Mg,Mn)Ge_2O_{7+\delta}$ includes the rarely found $Mn(3+)O_5$ trigonal bipyramid and the GeO_5 square pyramid, which were both induced by an interstitial oxygen atom. The blue color of the chromophore results from the d–d electronic transition in $Mn^{3+}(d^4)$, which has a trigonal-bipyramidal coordination. We proposed that the formation of $Mn(3+)O_5$ might be the result of the tendency to decrease the mismatch between the sizes of the $Mn(2+)O_4$–GeO_4 and SrO_8 layers in the layered melilite $Sr_2(Mn,Mg)Ge_2O_{7+\delta}$. The results of the analysis performed in the study suggest that such a layered-melilite structure, which has various isomorphs, could be used for controlling the coordinations or the valence states of transition metal ions.

Acknowledgements

The authors wish to acknowledge the contributions of Dr Byungki Ryu for his helpful advice about *ab initio* calculation. C. C. Lin and R.-S. Liu would like to acknowledge the financial support from the National Science Council of Taiwan under the contract number of NSC 101-2113-M-002-014-MY3.

References

1 M. Pastoureau, *Blue: The History of a Color*, Princeton University Press, 2001.
2 M. P. Shores, L. G. Beauvais and J. R. Long, *J. Am. Chem. Soc.*, 1999, **121**, 775.
3 R. Linguerri, N. Komiha, J. Fabian and P. Rosmus, *Z. Phys. Chem.*, 2008, **222**, 163.
4 M. Karmaoui, N. J. O. Silva, V. S. Amaral, A. Ibarra, Á. Millánc and F. Palacioc, *Nanoscale*, 2013, **5**, 4277.
5 A. E. Smith, H. Mizoguchi, K. Delaney, N. A. Spaldin, A. W. Sleight and M. A. Subramanian, *J. Am. Chem. Soc.*, 2009, **131**, 17084.
6 H. Mizoguchi, A. W. Sleight and M. A. Subramanian, *Inorg. Chem.*, 2011, **50**, 10.
7 S. Tamilarasan, D. Sarma, M. L. P. Reddy, S. Natarajan and J. Gopalakrishnan, *RSC Adv.*, 2013, **3**, 3199; D. A. Rusakov, A. A. Belik, S. Kamba, M. Savinov, D. Nuzhnyy, T. Kolodiazhnyi, K. Yamaura, E. Takayama-Muromachi, F. Borodavka and J. Kroupa, *Inorg. Chem.*, 2011, **50**, 3559.
8 L. Sacconi, *Pure Appl. Chem.*, 1968, **17**, 95.
9 H. Naruse, K. Tanaka, H. Morikawa and F. Marumo, *Res. Lab. Eng. Mater., Tokyo Inst. Technol., Rep.*, 1984, **1984**, 1.
10 T. Endo, Y. Doi, Y. Hinatsu and K. Ohoyama, *Inorg. Chem.*, 2012, **51**, 3572.
11 Y. Ochi, K. Tanaka, H. Morikawa and F. Marumo, *J. Mineral. Soc. Jpn.*, 1982, **15**, 331.
12 F. Izumi and T. Ikeda, *Mater. Sci. Forum*, 2000, **198**, 321.
13 P. Hohenberg and W. Kohn, *Phys. Rev.*, 1964, **136**, B864; W. Kohn and L. J. Sham, *Phys. Rev.*, 1965, **140**, A1133.
14 P. E. Blochl, *Phys. Rev. B: Condens. Matter Mater. Phys.*, 1994, **50**, 17953.
15 G. Kresse and J. Furthmuller, *Phys. Rev. B: Condens. Matter Mater. Phys.*, 1996, **54**, 11169; G. Kresse and J. Joubert, *Phys. Rev. B: Condens. Matter Mater. Phys.*, 1999, **59**, 1758.
16 J. P. Perdew, K. Burke and M. Ernzerhof, *Phys. Rev. Lett.*, 1996, **77**, 3865.
17 J. Lü, F. Du, R. Zhu, Y. Huang and H. J. Seo, *J. Mater. Chem.*, 2011, **21**, 16398; V. M. Khot, A. B. Salunkhe, M. R. Phadatare, N. D. Thorat and S. H. Pawar, *J. Phys. D: Appl. Phys.*, 2013, **46**, 055303.
18 J. E. Huheey, E. A. Keiter and R. L. Keiter, *Inorganic Chemistry: Principles of Structure and Reactivity*, Harper Collins, New York, 4th edn, 1993, pp. 439–440.
19 J. M. Alonso, R. Cortés-Gil, L. Ruiz-González, J. M. González-Calbet, A. Hernando, M. Vallet-Regí, M. E. Dávila and M. C. Asensio, *Eur. J. Inorg. Chem.*, 2007, 3350.
20 L. A. J. Garvie and A. J. Craven, *Phys. Chem. Miner.*, 1997, **21**, 191.
21 K.-W. Nam, M. G. Kim and K.-B. Kim, *J. Phys. Chem. C*, 2007, **111**, 749; F. Farges, *Phys. Rev. B: Condens. Matter Mater. Phys.*, 1996, **71**, 155109.
22 D. N. Sathyanarayana, *Electronic Absorption Spectroscopy and Related Techniques*, University Press, India, 2001, p. 272.
23 X. Kuang, M. A. Green, H. Niu, P. Zajdel, C. Dickson, J. B. Claridge, L. Jantsky and M. J. Rosseinsky, *Nat. Mater*, 2008, **7**, 498.
24 C. Tealdi, P. Mustarelli and M. S. N. Islam, *Adv. Funct. Mater*, 2010, **20**, 3874.
25 A. Mancini, C. Tealdi and L. Malavasi, *Int. J. Hydrogen Energy*, 2012, **37**, 8073.

